On the development of a low-cost lithographic interferometer

by

Hasan Korre

A.B., Physics, Harvard College (2009)

Submitted to the Department of Electrical Engineering and Computer Science
in partial fulfillment of the requirements for the degree of

Masters of Science in Electrical Engineering and Computer Science

at the

MASSACHUSETTS INSTITUTE OF TECHNOLOGY

September 2010

Author .....
Department of Electrical Engineering and Computer Science
September 3, 2010

Certified by .....
Karl K. Berggren
Associate Professor of Electrical Engineering
Thesis Supervisor

Accepted by .....
Terry P. Orlando
Chairman, Department Committee on Graduate Theses

On the development of a low-cost lithographic interferometer

by

Hasan Korre

Submitted to the Department of Electrical Engineering and Computer Science
on September 3, 2010, in partial fulfillment of the
requirements for the degree of
Masters of Science in Electrical Engineering and Computer Science

Abstract

Interference lithography is a technique for making one- and two-dimensional periodic nanostructures using interference of two coherent light beams. Despite their successes, the size, maintenance, and cost of interference lithography tools have prevented periodic nanostructures from being ubiquitous in academia and industry. Here, a novel approach is described whereby the conventional optical source – a bulky and expensive metal-vapor laser – is replaced by a newly available, low-cost blue laser diode. Additionally, the passive alignment of a lens tube is utilized to simplify the construction of a spatial filter. The resulting custom-built interference lithography tool is able to print large-area ($\sim$cm^2) periodic patterns. The tool has a small footprint ($\sim$0.2 m^2) and can be assembled for less than 6000 USD.

Thesis Supervisor: Karl K. Berggren
Title: Associate Professor of Electrical Engineering

Acknowledgments

First, I would like to thank Prof. Karl Berggren for giving me the opportunity to work in his group. Your vision for me and the project have been superb. Also, your advice, encouragement, and enthusiasm definitely have not gone unnoticed or unappreciated.

Furthermore, there are a lot of people who's expertise, guidance, and camaraderie contributed to my successful completion of this thesis and they deserve my gratitude.

To Corey Fucetola, who was there every step of the way. Thanks for being a great mentor and an even better friend. I couldn't have made it without you;

To Jeremy Johnson for his help in taking optical spectrum measurements. This project wouldn't have been possible without your generosity;

To Lin Lee Cheong for providing more hugs and chocolate than an officemate could ever ask for;

To Tim Savas for laser recommendations and optical advice;

To Jim Daley for all his help in the clean room and for keeping things lively around the lab;

To Tom O'Reilly for his help with optics setup and advice;

To Alicia Akins for administrative assistance and lively conversation. Never give up the search for the graviton!

To Jeffrey Moses for his mentorship. You have definitely made my first year of grad school memorable;

To Joy Johnson for being someone I could talk to when I just had no idea what I was doing;

To MIT Summer Research Program (MSRP) Staff including Dean Christopher Jones, Monica Orta, and Nancy Guilllen for allowing me to start my MIT journey through the program;

To Janet Fischer and Prof. Eric Hudson for helping bring me to the MSRP program;

To Prof. Isaac Chuang for teaching me what engineering is all about;

To Prof. Terry Orlando for his guidance as my academic advisor;

To Dr. Euclid Moon for writing tutelage.

To Prof. Henry Smith for his advice on the project;

To my labmates Diana Aude, Lorenzo Battistella, Jae-Byum Chang, Bryan Cord, Andrew Dane, Huigao Duan, Katherine Harry, Charles Herder, Xiaolong Hu, Joshua Leu, Vitor Manfrinato, Francesco Marsili, Adam McCaughan, David Meyer, Faraz Najafi, Vinay Ramasesh, Randy Peterson, Mike Snella, Sebastian Strobel, Donald Winston, and Joel Yang (Whew!) for their friendship;

And last but not least to my mother, father, sister and family for their continued encouragement and support. I can only hope that I will continue to make you all proud.

Contents

List of Figures

Chapter 1

Introduction

T plus 19,000 hours. We have thesis, Houston. We have thesis. Mission Control clapped and cheered and the engineers hugged one another and shook one anothers' hands and patted one another on the back and looked up at the large-screen television and tears welled up in more than one pair of eyes. The *Eagle* has landed.

Pepper White, Former MIT Graduate Student[1]

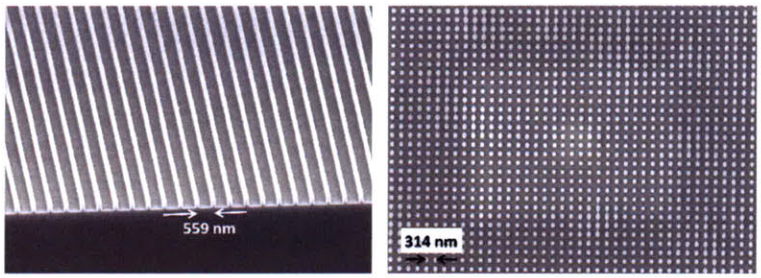

Figure 1-1: Scanning electron micrograph images of one- and two-dimensional nanostructures made with interference lithography.

Interference lithography (IL) has proven itself as an enabling technology for nanofabrication of periodic nanostructures. Within IL, issues of spatial phase distortion[2], fringe stability[3], and substrate development[4] have been explored and addressed. However, IL tools are still unnecessarily expensive, large, and complex. Here I present the basics of IL.

1.1 The Need for Low-cost Periodic Nanostrucutres

The term nanostructure refers to a feature in which at least one spatial dimension is < 1 μm. Periodic nanostructures contain a basic structure, such as a line or dot, repeated at constant intervals over a substrate. The periodicity can be in one, two, and possibly three dimensions. Figure 1-1 shows examples of one- and two-dimensional periodic nanostrucutres. Nanostructures with one dimension of periodicity are commonly referred to as *gratings* while nanostrucutres with two dimensions of periodicity are commonly called *rods* or *holes*.

Periodic nanostuctures have found a myriad of applications. They have proven useful as photonic crystals, diffraction gratings, magnetic domains in recording media, and nanochannels in microfluidics.[5] Recently, periodic nanostructures have also been adapted to create templates for self-assembly[6], to fabricate nanoimprint molds[7], to verify new lithographic techniques such as absorbance modulation[8, 9], and to influence the placement of extracellular matrix by osteoblasts[10]. Despite its suc-

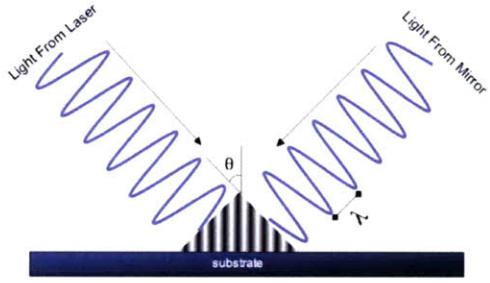

Figure 1-2: Schematic of interference lithography (IL). When two incident plane waves interfere, they create a sinusoidal intensity pattern that can be captured in photoresist.

cesses, the size, complexity, and cost of nanofabrication tools have prevented periodic nanostructures from becoming ubiquitous in labs, schools, and companies.

1.2 Interference Lithography

Interference lithography is a technique for making one- and two-dimensional periodic nanostructures by using interference from two coherent light beams. As shown in Fig. 1-2, when the two beams interfere at the substrate, they form a sinusoidal intensity pattern. This pattern can be captured in a photosensitive material called a photoresist. The latent intensity pattern in the photoresist can be revealed by using a liquid *developer*, in analogous fashion to photographic film. As a result, the transient, periodic intensity pattern is turned into a permanent, periodic topographical pattern.

The pitch, or spacing, of the resulting nanostructures is governed by a simple formula:

$$p = \frac{\lambda}{2\sin\theta}. \tag{1.1}$$

Here λ is the wavelength, and θ is the half angle between the two interfering beams. Often, researchers are interested in obtaining the smallest possible pitch. From Eq. 1.1, it is evident that a smaller pitch is achievable using smaller wavelengths and larger interference angles. Often, laser technology and the spectral sensitivity of

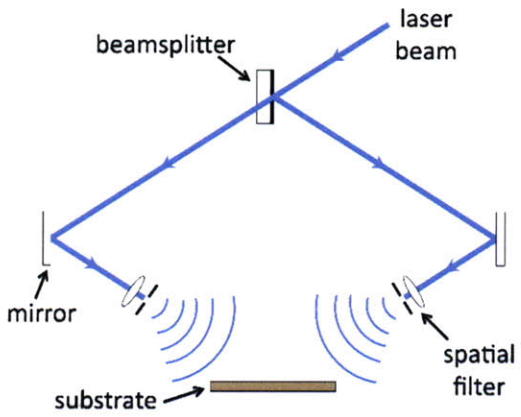

Figure 1-3: The Mach-Zehnder interference lithography system. A laser beam is split and then recombined as two spherical waves at a substrate.

the photoresist place a limit on the minimum wavelength. In this case, the pitch of the periodic pattern is primarily determined by the interference angle. The result is that the minimum pitch is $p_{min} = \lambda/2$.

The most well-know configuration of IL is the Mach-Zehnder interferometer (Fig. 1-3). In this setup, a collimated beam is split evenly by a beam splitter. The beams then individually bounce off mirrors and pass through spatial filters made of a lens and a pinhole. This creates two spherical waves that interfere at a substrate. With large beam-expansion lengths, the Mach-Zehnder can create large patterned areas with minimal spatial phase distortion.

The Mach-Zehnder suffers from issues of complexity. In order to change the pitch of the pattern, both beam arms must be repositioned and two sets of optics must be realigned. Also a phase error sensor and phase adjuster (e.g. Pockels cell) must be used. Once the initial beam is split in two by the beam splitter, the phase of each beam can be altered by mechanical vibrations and air turbulence. If the relative phase of the two beams is not locked, the interference fringes may "walk", causing the latent intensity pattern to be destroyed. Despite these challenges, the Mach-Zehnder interferometer is often the tool of choice for fabricating spatially coherent, periodic patterns.

Figure 1-4: Schematic of a Lloyds Mirror setup developed at MIT. The setup includes a laser, collimating lens, a lens/pinhole spatial filter, and a mirror/substrate chuck.

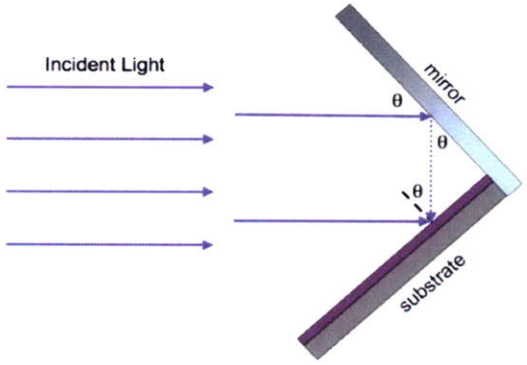

Figure 1-5: In a Lloyd's Mirror, reflection from a mirror causes interference at the substrate.

1.3 The Lloyd's Mirror

The Lloyd's mirror interference lithography configuration uses a simple and rigid setup to produce one- and two-dimensional nanoscale patterns. A typical Lloyd's mirror, like the one in the Nanostructures Laboratory at MIT[11, 3], consists of a collimated HeCd gas laser, a lens/pinhole spatial filer and a rigid mirror/substrate chuck. Figure 1-4 shows an example of such a setup. The benefit of the Lloyd's mirror configuration over other setups is that the rigidity of the mirror/substrate chuck reduces the effects of vibrations. Unlike the Mach-Zehnder, where the two beams of the interferometer are separated early, in the Lloyd's mirror the two beams are effectively created when the original beam reaches the mirror/substrate chuck. This makes the Lloyd's mirror very tolerant of vibrations and air turbulence, which would normally disrupt the phase of a Mach-Zehnder system.

Another benefit of the Lloyd's mirror is that it allows for simple modification of the pitch. Figure 1-5 is a schematic of the arrival of light at the mirror/substrate

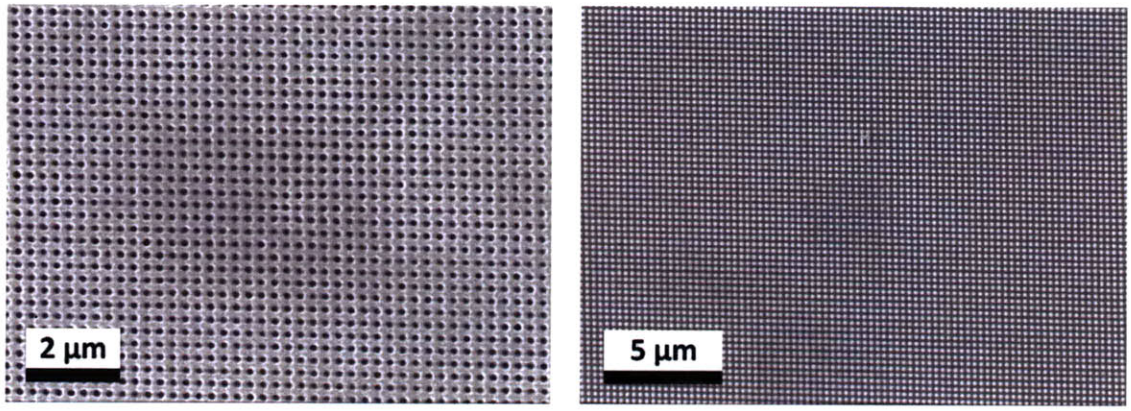

Figure 1-6: Scanning electron micrographs of two-dimensional nanostructures. Both patterns were formed using a double exposure technique.

chuck. Since the angle between the mirror and substrate is fixed at 90°, rotation of the chuck merely changes the interference angle at the substrate. This is in contrast to the Mach-Zehnder, which requires the realignment of two beam paths and the resulting two sets of optics.

The Lloyd's mirror is not without its faults. The most concerning issue is that the mirror comes after the spatial filter. As a result, any imperfections in the mirror – whether they are dust, scratches, or thickness changes – will be imaged onto the substrate. Also, the dimensions of the mirror limit the size of the wafer that can be exposed with the tool.

Two-dimensional rod and hole patterns can be created with a Lloyd's mirror using a double exposure technique. In the first exposure, half of the clipping dose (the dose at which a resist goes from unexposed to exposed) is applied. Then the substrate is rotated 90° and the other half of the dose is applied. Modifying the total dose applied or changing the resist type can allow the user to select a rod or hole pattern. Figure 1-6 shows examples of rods and holes in photoresist.

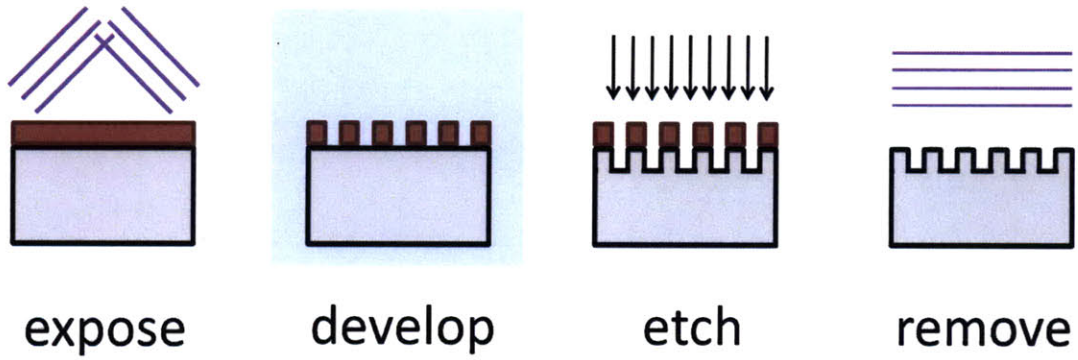

Figure 1-7: Creation of a periodic pattern in a functional material. The steps include: (a) UV exposure of a periodic pattern in photoresist, (b) liquid development of the pattern, (c) physical/chemical etching of the pattern into lower layers, and (d) removal of residual films.

1.4 Substrate Design and Processing

Sec. 1.2 describes how to form a periodic pattern in a photosensitive material, but often materials that are useful for devices are not photopatternable. As a result, patterns must be transferred from the photosensitive material to a device layer. Figure 1-7 shows a series of steps used to produce periodic nanostructures in a functional material. Interference lithography with UV light is used to produce a latent pattern in photoresist. The periodic pattern is revealed in a liquid developer. Then the pattern is transferred to the functional layer by physical or chemical etching. Finally, the residual films are removed by flood exposure, a solvent rinse, or a different etch process.

A key parameter during interference lithography is the exposure time. The exposure time can be derived from the incident intensity (incident power/detector area) and the clipping dose. Exposure times for different angles can be calculated using the formula

$$t = \frac{D_0}{I_p T(1+R)\cos\theta}, \tag{1.2}$$

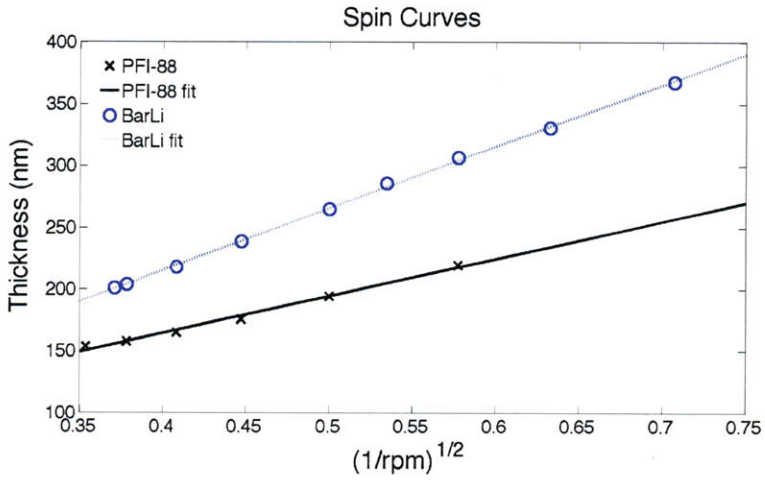

Figure 1-8: Spin curves for PFI-88 photoresist and Barli antireflection coating. Spin speeds were used on a wafer spinner, while thickness data comes from an ellipsometer.

where t is the exposure time, D_0 is the clipping dose, I_p is the incident laser intensity, T is the proportion of light transmitted through the resist, R is the fraction of light reflected back into the resist, and θ is the beam angle at the substrate.[12]

Generally, one does not place photoresist directly on top of a device material. At the interface of two substrate layers there are reflections of the incident light as a result of the differing indexes of refraction of the materials. The incident and reflected light can form a sinusoidal interference pattern that travels vertically into the photoresist. If this happens, the resulting nanostructures will have verticlal ripples in their sidewalls called standing waves.[4] Materials called antireflection coatings (ARC) minimize this effect by having an index of refraction that closely matches the index of refraction of the photoresist. ARCs also absorb much of the residual light that is not absorbed by the photoresist, minimizing the risk of additional reflections from the device layer.

The effectiveness of an antireflection coating at preventing standing waves is very dependent upon the thickness of the photoresist and ARC layer. This is because the phase difference between light reflecting from each layer interface can increase or decrease the severity of standing waves. Both photoresist and ARC are spin coated onto substrates. A spin curve was developed by performing a linear fit to data of

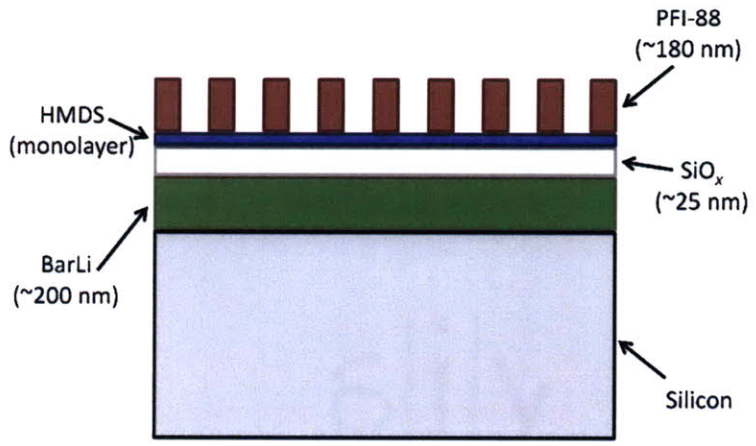

Figure 1-9: A silicon substrate with a trilayer stack used for interference lithography. The stack consists of a photoresist (PFI-88), an inner layer (SiOx), and an antireflection coating (BarLi). An adhesion promoter (HMDS) is used to adhere the photoresist to the inner layer.

the layer thickness and the square root of the spin speed.[1] The spin speed was an independent variable given to a wafer spinner, while the thickness was measured on an ellipsometer. The graph is plotted in Fig. 1-8.

After a latent pattern is developed, that pattern must be transferred to the underlying device material. Although there are a few ways to accomplish this, often reactive-ion etching is done. During reactive-ion etching, a plasma chemically reacts with the substrate yielding volatile products that desorb from the surface. Concurrently, ion bombardment creates anisotropy in the etch, which is important for developing vertical sidewalls. Typically an inner layer is added to provide good etch selectivity between a patterned layer and the device layer. Etch selectivity refers to the ratio of the speeds of material removal for two different layers. An example of an inner layer is the use of silicon dioxide (SiO_x) with a silicon device layer. If one were to simply try to etch down into silicon without the SiO_x inner layer, the photoresist pattern may etch away before it is transferred into the silicon. The combination of a photoresist, an inner layer, and an antireflection coating is reffered to as a trilayer stack (Fig. 1-9).[4]

[1]The fit was done by Corey P. Fucetola.

Chapter 2

Blue Laser Diodes as Sources for Interference Lithography

We would find it hard to remove any given button from a DVD player if forced to do so. The problem is one of choosing what deserves to live, at the sacrifice of what deserves to die. Such decisions are not easy...

John Maeda, Former MIT Professor of Media Arts & Sciences[13]

Interference lithography (IL) systems generally exist in larger well-equipped laboratories, where their ~50 000 USD price tag is not a substantial constraint. These tools are designed to pattern periodic structures over large areas (>1 mm^2) for applications such as spectroscopy, magnetic storage, and nanofabrication process development.[3] However, some of these applications, such as nanofabrication process development, do not require large grating areas. Hence, there also exists a need for <1 mm^2 area patterning in a variety of smaller laboratories and educational facilities that is not being met in part due to cost, access, infrastructure, and maintenance requirements of existing IL tools.

The goal of the project was to lower the cost of IL by substitution of newly-available, low-cost blue laser diodes for the more commonly used HeCd laser. The concept of using 405 nm light from solid-state sources is not new. Some examples of lithography tools that use 405 nm diodes as light sources have recently been reported. In 2003, a blue diode laser was used to write 130-nm-wide pits in a read-only memory disk.[14] In 2006, Heidelburg Instruments produced a 1 μm linewidth direct-write diode-laser-based pattern generator.[15] In 2008, an UV-light emitting diode optical-projection lithography system capable of 2 μm linewidth was presented in the 34th Micro and Nano Engineering Conference.[16] However, use of these sources for IL had not been reported.

2.1 The Tiny Lloyd's Mirror

2.1.1 Setup

Figure 2-1 shows two varieties of a Lloyd's mirror interferometer. In Fig. 2-1(a) is shown a conventional Lloyd's mirror lithography system used to pattern samples with areas larger that 1 cm^2, which requires: a laser source with adequate temporal coherence length and wavelength under 500 nm, a collimating lens, a spatial filter, a long beam-expansion region, and a mechanically rigid rotatable mirror and sample holder. In Fig. 2-1(b) is the simplified version called the Tiny Lloyd's Mirror (TLM).[1] The

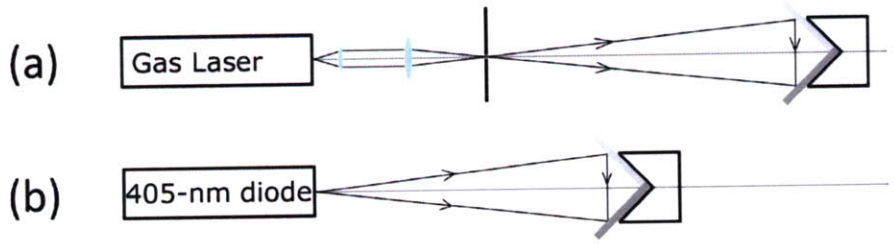

Figure 2-1: Two configurations of the Lloyd's mirror lithography system: (a) includes a collimated, long coherence length source and spatial filter upstream of the mirror/substrate chuck to improve the beam quality and (b) includes both an inexpensive 405 nm diode laser and an inexpensive mirror/substrate chuck. In (a), the mirror/substrate chuck holds both a mirror and substrate in a perpendicular orientation, which can be rotated to control the pattern pitch. In (b), the same configuration is chosen but the chuck is fixed, the spatial filter is removed, and the gas laser is replaced by a 405 nm diode laser. The distance between the laser and stage was ~25 cm; the mirror was 2×4 cm^2 and the substrates were quarter wafers approximately 812 cm^2 in area.[17]

initial goal of the project was to pattern ~1 mm^2 area; therefore, only the essential elements from a conventional Lloyd's mirror were retained. Elements which aided the achievement of a large patterning area or a tailored pitch were deemed unnecessary at this point and were eliminated. This simplified version uses only an inexpensive 405 nm diode laser and a machinist's block for holding the mirror and sample. The only optical elements in this tool are the diode facet and a Cr mirror. The core requisite feature of the interferometer, that it generates subwavelength optical patterns, is retained in both approaches.

Figure 2-2 shows a picture of the Tiny Lloyd's Mirror which was made of (1) an optical source and (2) a machinist's block. The source consisted of a 5 mW 405 nm wavelength diode laser module, which was $\sim 5\times$ cheaper than a single-mode diode. The source was aligned using a collimating lens. A prism polarizer cut at the Brewster angle was used to set the incident polarization at the mirror and sample to s-polarization, or equivalently, the electric field was set perpendicular to the mirror's

[1] *The Tiny Lloyd's Mirror* is a name coined by Corey P. Fucetola in a final paper for the 6.781 class at MIT.[18] In addition, much of the work to develop the Tiny Lloyd's Mirror was done with the assistance and guidance of Fucetola.

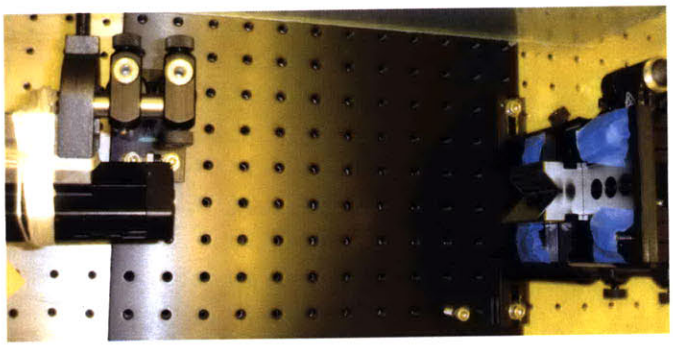

Figure 2-2: Picture of the Tiny Lloyd's Mirror. On the left is a laser diode module including a blue laser diode and current drive electronics. On the right is a stainless steel v-block which holds the mirror and substrate.

plane of incidence (and hence parallel to the grating lines). The polarizer and lens were then removed prior to sample exposures so that the elliptically shaped, diverging light emitted from the diode had the short axis of the ellipse aligned parallel to the grating lines. The machinist's block held a mirror consisting of a silicon wafer coated by electron-beam evaporation with 25 nm of chrome on one of its faces, mounted with two-sided adhesive carbon tape. The mirror's reflectivity was measured for 45° incident, s-polarized, light to be 76.5%. On the perpendicular face, the block held the sample, also mounted with two-sided adhesive carbon tape, so that the edge of the sample was nested behind the mirror edge. The block was separated from the source by ~25 cm.

A fabrication process was developed for the samples consisting of application of a trilayer resist stack, optical exposure, and development. Wafers were coated with a resist stack[4] consisting of three separate layers: (1) an antireflection coating (ARC) (AZ Electronic Materials, Barli) applied by spin coating at ~7.28 krpm to achieve a 200 nm thickness, followed by baking on a hot plate at 175°C for 90 s, (2) 25 nm of SiO_x deposited in an electron-beam evaporation system with thickness controlled using in situ quartz crystal monitor, and (3) a positive-tone photoresist (PFI-88, Sumitomo Chemicals) spin coated at ~3.8 krpm to achieve an estimated thickness of ~180 nm and then baked on a hot plate at 110°C for 90 s. The SiO_x interlayer is incorporated into the resist stack for postlithographic processing, wherein it masks

the ARC during subsequent etch transfer steps. After deposition of the SiO_x but before application of the photoresist, wafers were coated with a layer of hexamethyldisilazane (HMDS) by spin coating using the following procedure: (1) application of HMDS from a plastic pipette to coat the sample surface, (2) a delay of 60 s to allow for bonding of the HMDS layer, (3) 5 s spinning at ~3.8 krpm, and (4) delay in ambient environment of ~5 min before further processing to permit the surface to fully dry. After application of photoresist, the wafers were cleaved into quarters, forming ~812 cm^2 pieces used for individual exposure experiments. Optical dose was controlled by using a simple shutter to unblank the optical beam for a timed period. Typical exposure times were ~2530 s, and the optical power was ~5 mW. Samples were developed by liquid immersion in 0.26N (2.4% wt) tetramethylammonium hydroxide developer (CD-26, Rohm & Haas Electronic Materials) for 60 s, then immersed in de-ionized water, and finally blown dry using dry N_2 gas.

After processing, samples were inspected visually with the naked eye, and then inspected closely by scanning-electron microscopy (SEM). The SEM was calibrated by using an image of a standard grating. Prior to SEM inspection, samples were coated by sputter deposition of < 5 nm of Au/Pd to prevent charging. The scanning-electron microscope imaging was performed on a DSM 982 Gemini SEM column from Zeiss SMT, with an in-lens secondary-electron detector, at 5 keV with a 7 mm working distance.

2.1.2 Results

The Tiny Lloyd's Mirror was able to fabricate ~300 nm pitch gratings. Figure 2-3 shows scanning electron micrograph images of one-dimensional nanostructures in photoresist. The system, which cost less than 1000 USD, was able to produce nanoscale features with steady linewidth (no pinching) and without footing.

Although the Tiny Lloyd's Mirror was able to produce periodic nanostructures, complications arose. The gratings were limited to ~1 mm^2 of continuous area. Moreover, the diffraction gratings produced by this tool had nonuniformities that were visible to the naked eye. Figure 2-4 is a picture of diffracted light from a substrate

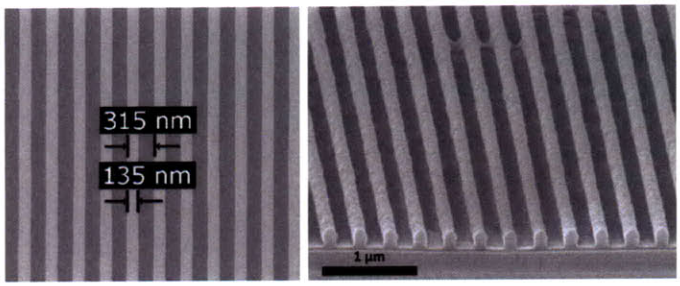

Figure 2-3: Scanning electron micrographs of one-dimensional nanostructures in photoresist made with the Tiny Lloyd's Mirror.[17]

Figure 2-4: Substrate with a spatial beating pattern. The stripes are diffracted light from one-dimensional nanostructures.

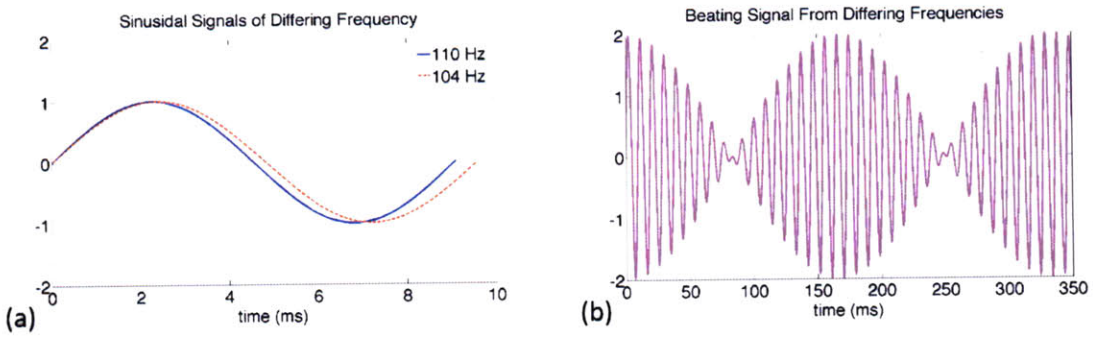

Figure 2-5: Beating. (a) Two sinusoidal signals of differing frequency. (b) The sum of the two signals. There is an envelope modulating the sinusoid.

that was patterned with the Tiny Lloyd's Mirror. Instead of a continuous area of diffraction, the result was strips of patterned area that appeared periodically on the substrate traveling perpendicular from the mirror edge.

The result can be explained as a beating pattern. Figure 2-5 gives a graphical depiction. When two sinusoidal signals of close frequency sum together, they create a signal with an envelope:

$$\sin(2\pi f_1 t) + \sin(2\pi f_2 t) = 2\cos(2\pi \frac{f_1 - f_2}{2} t)\sin(2\pi \frac{f_1 + f_2}{2} t). \tag{2.1}$$

The cosine term is of low frequency: $f_{beat} = (f_1 - f_2)/2$. In Fig. 2-5(a) there are two sine waves of close frequency. In Fig. 2-5(b) their sum is graphed.

2.2 Temporal Coherence

Temporal coherence is a correlation of the phase and wavelength of a wave at different times. Practically, a temporally coherent source can interfere with a delayed version of itself (e.g. Michelson interferometer). A monochromatic source is temporally coherent because (1) there is a fixed relation between the initial phase and final phase and (2) the initial and final wavelength are known. As a result, sources that work through stimulated emission (which conserves phase) and sources which have a narrow spectrum are considered temporally coherent.

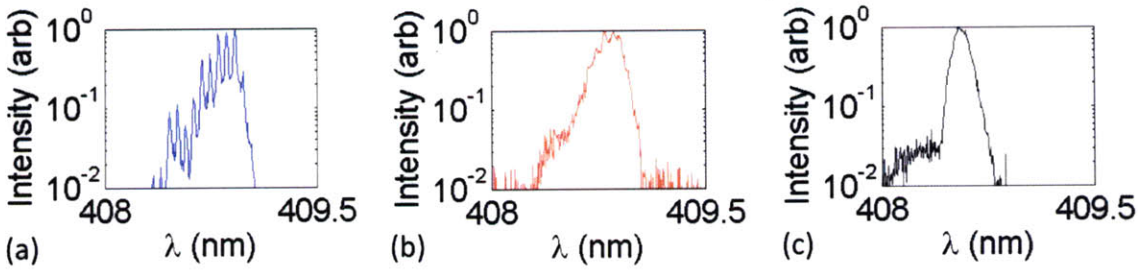

Figure 2-6: Spectral measurements from the laser diode module. Each measurement was taken on different days, separated by several weeks.[17]

The characteristic time over which a wave can interfere with a delayed version of itself is called the coherence time. By multiplying the coherence time by the speed of light, one can calculate the coherence length. In the Lloyd's mirror interferometer, the beam that bounces off the mirror travels a longer distance than the beam that travels directly toward the substrate. When the difference in path length between the two beams is longer than the coherence length, interference cannot occur; the sinusoidal intensity pattern needed to form periodic nanostructures will not be created.

In order to identify the source of the beating pattern, spectra of the blue laser diode were taken. We used a spectrometer to record the optical output spectrum of the laser prior to exposing samples. The spectra were measured using a Spectrex spectrometer with 5.5 pm spectral resolution.[2] Figure 2-6 shows three spectral measurements of the laser module. The spectra differ because the spectrum of the laser module was found to drift with use. Note that Fig. 2-6(a) clearly shows multiple spectral modes while Fig. 2-6(b) and (c) show a more continuous spectrum.

Fringe visibility, or fringe contrast, is an important metric for interference lithography. Fringe visibility is a measure of the contrast of a spatially dependent intensity distribution. We define the fringe contrast of a sinusoidal signal by the equation:

$$contrast = \frac{max - min}{max + min}. \tag{2.2}$$

[2]These measurements were done with the assistance of Jeremy A. Johnson, who setup and operated the optical spectrometer and measurement software.

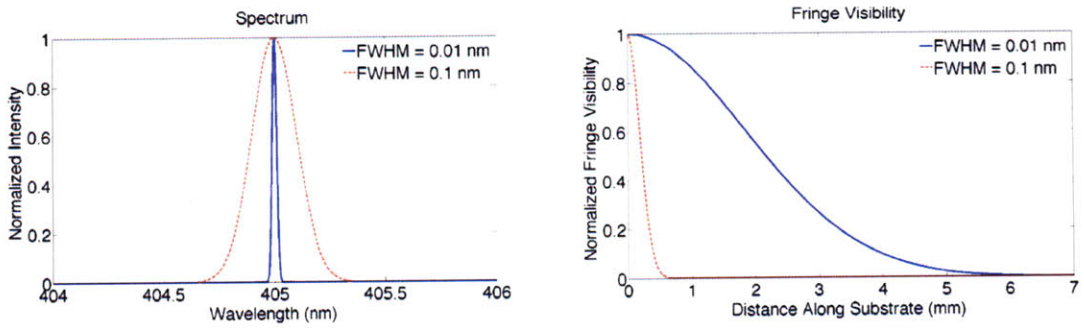

Figure 2-7: Theoretical Gaussian spectrums having different full width at half maximum and calculated fringe visibility.

For a sinusoidal intensity pattern, low fringe contrast is problematic because it decreases process latitude. With low contrast, the resulting pitch is very susceptible to changes in exposure dose.

The fringe contrast can be calculated [from the measured source spectrum] as a function of grating position by using the equation,

$$V(\Delta L) = \left| \int_0^\infty I(\nu) e^{-i2\pi\nu\Delta L/c} d\nu \right|, \tag{2.3}$$

where ΔL is the optical path difference between the two arms of the interferometer.[19] The optical path difference can be related to the distance x from the intersection of the mirror with the sample surface by using the equation:

$$x = \Delta L \frac{\sin\theta}{(1+\cos(\pi - 2\theta))}. \tag{2.4}$$

where θ is found from Eq. 1.1.

Figure 2-7 and 2-8 show the calculated fringe visibility for theoretical spectra. In Fig. 2-7(a) are two gaussian, single-mode spectrums of different width, and Fig. 2-7(b) shows their calculated fringe visibility. From these we can see that a narrower spectrum is desirable as it produces high fringe visibility over a longer distance. Figure 2-8 shows the effects of multi-mode spectra. All modes are Gaussian with FWHM = 0.01 nm. First, we notice that having multiple modes causes a beating

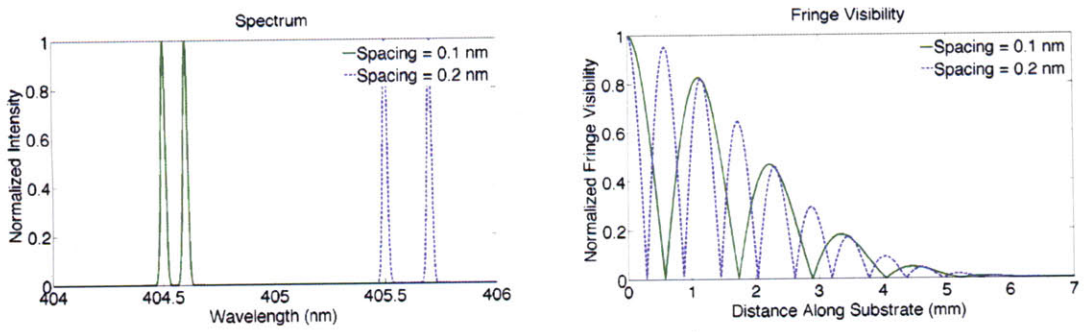

Figure 2-8: Theoretical Gaussian spectrums of different mode spacings and calculated fringe visibility. The solid graph in (a) is of two peaks spaced 0.1 nm apart. In the dotted graph, the peaks are spaced 0.2 nm apart. All mode have a FWHM of 0.01 nm.

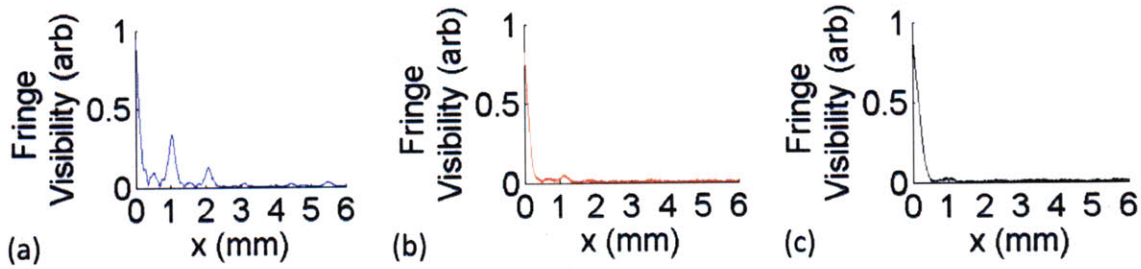

Figure 2-9: Calculated fringe visibility from the spectrums in Fig. 2-6 projected onto the wafer surface. The incident angle during the exposure was calculated from Eq. 1.1 using pitch measurements from SEM images. The angle was used to project the fringe visibility onto the surface of the substrate through Eq. 2.4.[17]

pattern in the fringe visibility but does not decrease the distance x over which gratings might be achieved ($\sim$6 mm). Second, closely spaced modes produce beats that are spaced farther apart.

Figure 2-9 shows the calculated fringe visibility from the measured spectrums of Fig. 2-6.[3] Figure 2-9(a) shows a considerable beating pattern. This result was expected since Fig. 2-6(a) was multimode. On the other hand, Fig. 2-9(b) and (c) lack a clearly visible beating. Also, the fringe contrast for (b) and (c) drop off very quickly, which is a result of their broad spectrums.

[3]These calculations were performed by Fucetola.

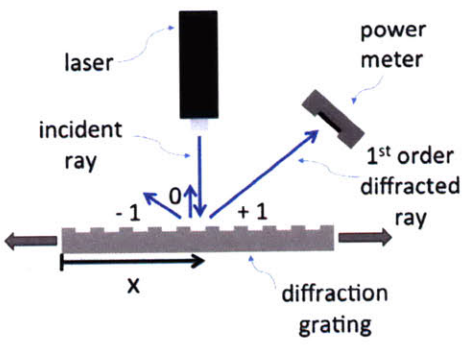

Figure 2-10: Schematic of setup used to measure the first-order diffracted power from fabricated gratings. The spatial variation in grating quality is mapped by translating the substrate and capturing the first-order diffracted ray.

2.3 Diffraction Efficiency

In order to get a quantitative measurement of the beating on the substrate, samples were evaluated by using a custom-built apparatus to determine the variation in diffraction efficiency across the sample. In this experiment, the fabricated sample was placed on a linear translation stage and illuminated with a 405 nm optical beam with a diameter of 82 μm at the substrate. The sample was aligned so that the grating lines were perpendicular to the direction of stage motion and to the laser's plane of incidence. A power meter was then placed in the path of the first-order diffraction spot. The reading on the power meter was recorded as a function of stage position in order to determine the positional dependence of the diffraction efficiency across the sample. Figure 2-10 shows a schematic of the setup.

In Fig. 2-11 is shown the measured first-order diffracted power from substrates (a)-(c). Both the measured diffraction efficiency and the fringe visibility of substrate (a) displayed a beating periodcity of $\sim$1 mm. The fringe visibility calculations for substrates (b) and (c) showed a single peak and their first-order intensity plots looked qualitatively similar. From the previous results, we surmised that the beating problem on the substrate was the result of a lack of temporal coherence from the laser.

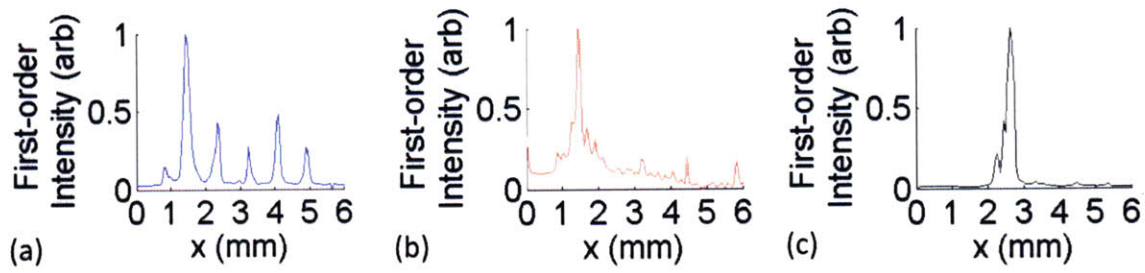

Figure 2-11: Measured first order diffracted power from gratings produced with the spectra in Fig. 2-6.[17]

2.4 Summary

The pivotal result of this chapter was the demonstration of ~300 nm pitch patterning capability at low cost. For less than 1000 USD, the Tiny Lloyd's Mirror was able to print grating lines. The capabilities and accessibility of this tool suggested that 405 nm diode lasers could be used as sources for interference lithography in both laboratory and educational settings. Although the substrates displayed non-uniformities, the cause was discovered to be the multimode nature of the laser spectrum. As a result, the key to realizing cm^2 or larger patterning areas is primarily improving the coherence length of the source. This can be simply accomplished either by purchasing single-mode sources or by using optical feedback from an external cavity to suppress additional modes.

Chapter 3

Optical Feedback

Like any engineering endeavor, nanofabrication is fundamentally about control and control requires feedback.

Karl K. Berggren, MIT Associate Professor of Electrical Engineering and Hank I. Smith, MIT Professor of Electrical Engineering[20]

In Ch. 2, I was able to show that blue laser diodes could be used to make periodic nanostrucutres. I also found that the patternable area was limited by the temporal coherence of the laser, which is dictated by the laser spectrum. In this chapter, I explore methods to narrow the spectrum of blue laser diodes. Specifically, I present the use of Fabry-Perot etalons and volume holographic gratings as optical feedback elements.

3.1 Fabry-Perot Etalons

A Fabry-Perot etalon is an optical spectral filter based upon multiple internal reflections of light. Light that enters an etalon is filtered so that certain wavelengths have higher amplitude of reflectance than others. Laser diodes respond to light that enters their front facet by stimulating the emission of more photons of that wavelength. Thus etalons can be used to spectrally filter the emission of laser diodes and reflect that light back into a laser diode, causing an optical feedback effect. It has previously been shown that optical feedback from an etalon can narrow the spectrum of semiconductor lasers.[21, 22] I chose this method to show that it is possible to simply and cheaply modify the spectrum of blue laser diodes in order to eliminate the beating pattern seen in Ch. 2.

The spectral filtering properties of etalons is a result of multiple internal reflection that occurs within an etalon. Figure 3-1 shows a diagram. Assume monochromatic plane waves impinge on an etalon of index of refraction n_e. The plane waves were originally in a medium of index n_a and had amplitude E_0. The complex amplitudes of reflectance and transmittance for rays approaching a surface from outside the etalon are r and t. Likewise, the reflectance and transmittance for rays approaching a surface from inside the etalon are r' and t'. The amplitude of the reflected waves are then:

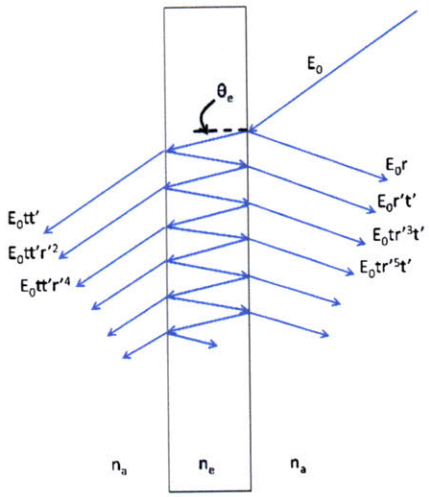

Figure 3-1: Multiple internal reflection inside a glass Fabry-Perot etalon. Adapted from Ref. [23].

$$
\begin{aligned}
E_{1r} &= E_0 r e^{i\omega t} \\
E_{2r} &= E_0 t r' t' e^{i(\omega t - \delta)} \\
E_{3r} &= E_0 t r'^3 t' e^{i(\omega t - 2\delta)} \\
&\vdots \\
E_{Nr} &= E_0 t r'^{(2N-3)} t' e^{i[\omega t - (N-1)\delta]},
\end{aligned}
$$

where δ is the phase that arises from the optical-path length between adjacent rays:

$$
\begin{aligned}
\delta &= k_0 \Lambda \\
k_0 &= 2\pi/\lambda_0 \\
\Lambda &= 2 n_e d \cos\theta_e,
\end{aligned}
\tag{3.1}
$$

where k_0 is the free space wave number, Λ is the optical path length between adjacent

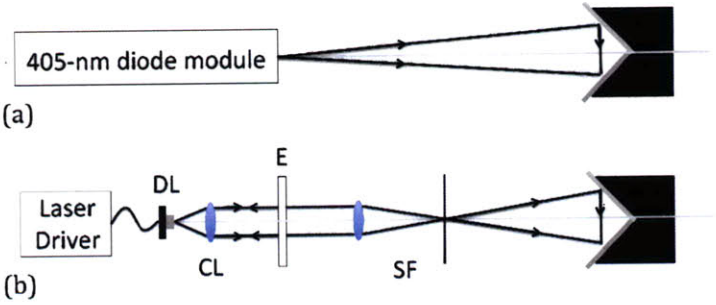

Figure 3-2: Two configurations of the Lloyd's mirror lithography system: (a) The Tiny Lloyd's Mirror. (b) A new Lloyd's mirror including a laser diode with a current driver, a collimating optic, an etalon, a spatial filter, and a mirror/substrate chuck.

rays, d is the thickness of the etalon, and θ_e is the angle of the rays inside the etalon. The resultant reflected scalar wave is:

$$E_r = E_{1r} + E_{2r} + E_{3r} + \cdots + E_{Nr}.$$

Using the geometric series and Stokes Relations for zero absorption, the reflected intensity from the etalon is [23]:

$$I_r = I_i \frac{F \sin^2(\delta/2)}{1 + F \sin^2(\delta/2)} \tag{3.2}$$

where we define $I_r = |E_r|^2/2$, $I_i = |E_0|^2/2$, and F is defined as the coefficient of finesse:

$$F = \left(\frac{2r}{1 - r^2}\right)^2.$$

Since $\delta \propto 1/\lambda$, we see from Eqn. 3.2 that the reflected intensity is a function of wavelength. The maximum of the function is $I_i[F/(1 + F)]$ and the minimum is 0.

In order to test etalons as optical feedback elements, I developed a Lloyd's mirror IL setup that incorporated an etalon. Figure 3-2 shows the original Lloyd's mirror setup and the modified setup including reflectance feedback from an etalon and beam shaping from a spatial filter. The etalon was a 0.5-mm-thick fused silica pellicle. Its reflectance spectrum is shown in Fig. 3-3 along with the reflectance for other

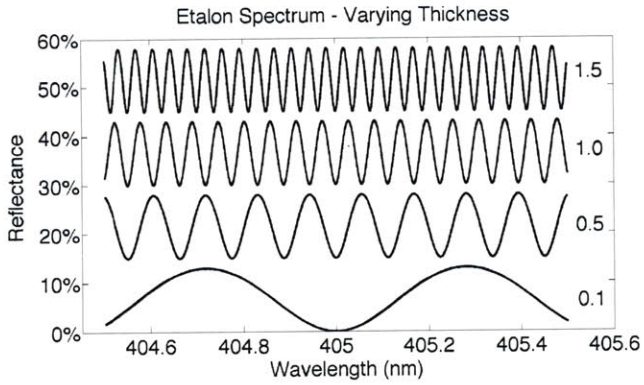

Figure 3-3: Calculated Reflectance Spectrum of fused silica etalons of differing thickness. The calculations are for 0.1, 0.5, 1.0, and 1.5-mm-thick etalons. The 0.5, 1.0, and 1.5 mm spectra have been shifted upward for clarity.

thicknesses. 0.5 mm was chosen because its free spectral range (112.5 pm) was roughly twice the spacing of peaks in a bare blue laser diode spectrum (50 pm for the Sharp GH04020B2A). I believed the etalon would select for the largest peak in the laser spectrum and reject the neighboring peaks.

The laser was collimated. Then the polarization was set using a Brewster's angle prism, and the laser was aligned to the v-block. The back-reflection from the etalon was aligned to the laser diode using a photodetector and oscilloscope. First, the etalon was roughly aligned by eye. Before alignment, two beams could be seen exiting the etalon. The etalon was tilted using a kinematic mount until the two beams roughly overlapped. Then the laser drive current was linearly ramped, and the laser power was measured by a photodiode and monitored on an oscilloscope. I manually aligned the etalon by observing a decrease in the threshold current as the laser achieved optical feedback. Finally, a spatial filter cleaned up the spatial coherence of the beam.

Figure 3-4 shows measured spectra of the blue laser diode in etalon feedback.[1] In (a), the spectrum of the laser before and after etalon feedback is shown. The spectrum after feedback is considerably narrower. The FWHM of the unfiltered spectrum is 2.01 nm, while the FWHM of the spectrum with etalon feedback is only 0.03 nm.

Unfortunately, the resulting spectrum after etalon feedback was not consistent.

[1]These measurements were done with the assistance of Jeremy A. Johnson.

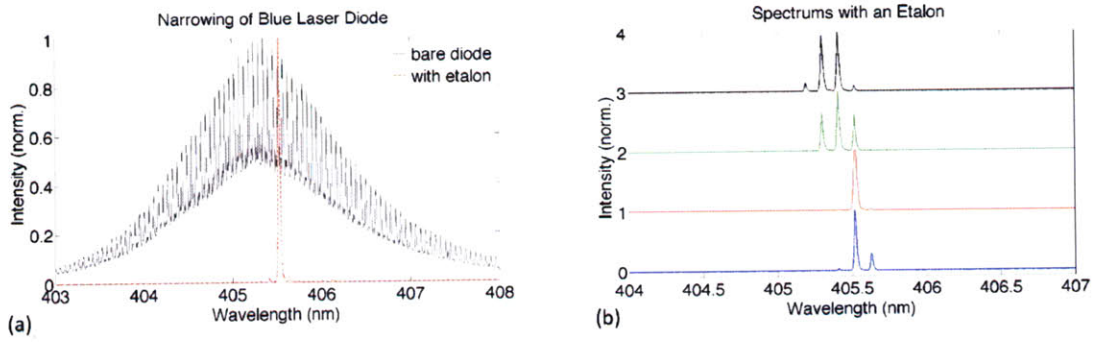

Figure 3-4: Measured blue laser spectral data before and after optical feedback from a Fabry-Perot etalon. (a) Change in spectrum due to an etalon. (b) Spectral measurements after multiple realignments of the etalon.

Figure 3-4(b) shows multiple spectrum measurements after aligning and realigning the etalon each measurement within a few minutes of the previous one. From the figure, it can be seen that the number of modes from the laser is not consistent. As was explained in Sec. 2.2, if the laser cannot be made single mode, the fringe contrast will display beating.

Faced with this problem, I explored ways to tune the spectrum of the etalon through changes in angle. The reflected intensity depends upon three factors: I_i, r, and δ. Two of these, r and δ, have angular dependence. δ is proportional to $\cos\theta_t$. r is angle-dependent due to the Fresnel Equations.[24] For TE polarization we have:

$$r_{TE} = \frac{n_1 \cos\theta_1 - n_2 \cos\theta_2}{n_1 \cos\theta_1 + n_2 \cos\theta_2}, \quad t_{TE} = 1 + r_{TE}.$$

And for TM:

$$r_{TM} = \frac{n_1 \sec\theta_1 - n_2 \sec\theta_2}{n_1 \sec\theta_1 + n_2 \sec\theta_2}, \quad t_{TM} = (1 + r_{TM})\frac{\cos\theta_1}{\cos\theta_2},$$

where the light is going from medium 1 to medium 2, and θ_2 can be found from Snell's Law. As a result of the Fresnel Equation, the reflectance is not only angle dependent but also polarization dependent. For IL, the laser polarization is oriented along the axis between the mirror and substrate. So, TE is for etalon rotation about its own y-axis, while TM is for etalon rotation about its x-axis.

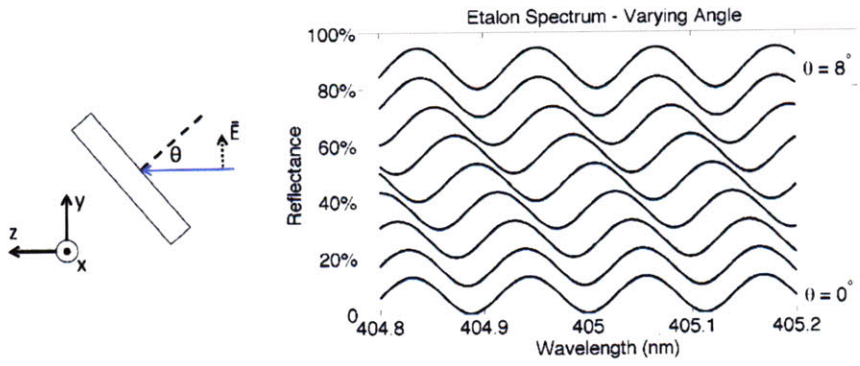

Figure 3-5: Calculated reflectance spectrum of a 0.5-mm-thick etalon for varying incident angles. Spectrums have been shifted upward for clarity.

In Fig. 3-5, I plot the TE etalon reflectance spectrum for changes in angle. The peaks in the spectrum shift smoothly as the incident angle increases. Unfortunately, angles of this magnitude were not achievable in my setup. The feedback would only stay aligned to the laser diode for very small angles. The smallest reasonable change in angle which could be achieved was $\Delta\theta = 0.64$ mRad ($\sim 0.02°$). It was only possible to rotate the etalon $\sim 3\Delta\theta$ before feedback was lost. For angles this small, there is almost no change in the etalon reflectance spectrum.

3.2 Volume Holographic Gratings

A volume holographic grating (VHG) is an optical element used to spectrally and spatially filter light. To construct a VHG, an interference pattern is captured in a thick hologram. Because the hologram is thick, Bragg diffraction occurs. According to Bragg's law,

$$2n\Lambda \sin\theta = m\lambda, \tag{3.3}$$

diffraction will only occur inside a medium at certain wavelengths ($m\lambda$) and certain angles (θ) given a grating spacing (Λ) and index of refraction (n).

Reflection VHGs are used as optical feedback elements similarly to how the etalon

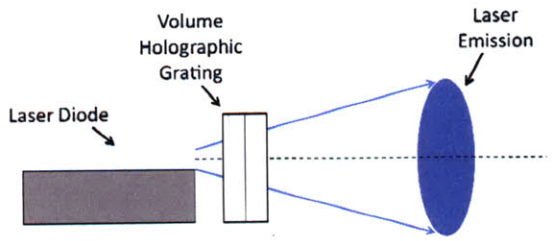

Figure 3-6: Setup of blue laser diode with a volume holographic grating in front for optical feedback. Redrawn from [25]

was used in Sec. 3.1. Incident light from a laser diode can be spectrally and spatially filtered by a VHG. The light would then be reflected back toward the diode. Only light of a narrow enough angle will arrive back at the laser diode facet and couple back into the diode. By Eqn. 3.3, the narrow angle spread will contain a narrow spectral bandwidth. As a result, the laser will begin to emit only the narrow band of wavelengths it receives from the VHG. Figure 3-6 shows a diagram of a laser diode in optical feedback from a VHG.

VHGs have advantages over Fabry-Perot etalons. Although both spectrally filter light into multiple wavelengths, the added spatial selectivity of the VHG allows for the selection of a particular wavelength. Also, VHGs have high diffraction efficiency and their spectral response is stable over the temperature range of 25–40°C.[25] Lastly, VHGs can be placed directly in front of a laser diode, allowing for compact packaging.

I used a commercially available 12 mW, 405 nm laser diode package with an integrated collimation and VHG optical feedback system.[2] Figure 3-7(a) shows the measured spectrum of the blue laser diode with optical feedback. Compared to the spectrum of the previous, unfiltered laser diode[17], the new spectrum is much narrower and displays fewer modes. A narrow spectrum should result in a longer coherence length and high intensity contrast over a large area. The calculated coherence length of the laser ($\sim \lambda^2/\Delta\lambda$) was estimated to be ~5.7 cm.

Figure 3-7(b) presents the measured first-order diffraction efficiency from a grating

[2]The spectrum data was supplied by Ondax, Inc. It was measured with an EXFO WA-1500 wavemeter using a WA-650 interface.

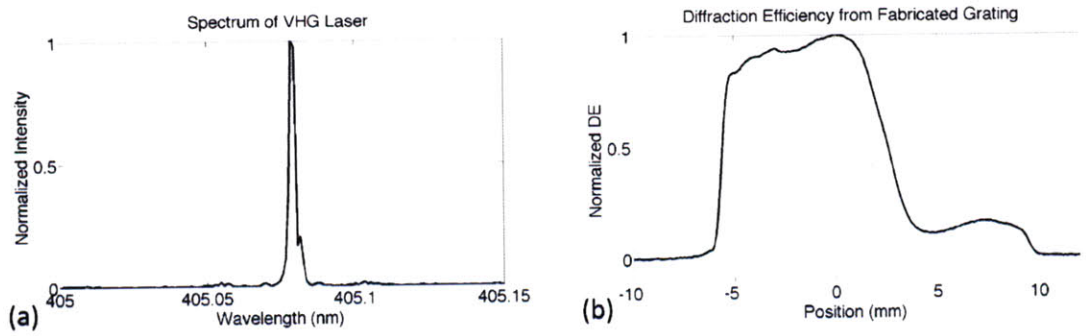

Figure 3-7: Temporal coherence investigation. (a) Spectral measurements from a laser diode with grating optical feedback using a spectrometer. (b) Measured first-order diffraction efficiency from a fabricated grating. The measurements were done by a home-built, automated setup. The diffraction efficiency is notably missing the $\sim$ mm scale beating pattern that was observed in Chapter 2.[26]

fabricated with the laser. The diffraction efficiency lacks the $\sim$ mm scale beating pattern seen in Ref. [17] and has a sharp drop off, which is believed to be due to the incident intensity variation produced by the spatial filter. Notably the normalized diffraction efficiency is continuously greater than 0.5 over 8 mm. This sample was observed to diffract light from an area larger than 1 cm^2.

3.3 Summary

In this chapter, Fabry-Perot etalons and volume holographic gratings were investigated as optical feedback elements. Using a 0.5-mm-thick fused silica etalon, I was able to narrow the full-width at half-maximum of the laser spectrum from 2.01 nm to 0.03 nm. Unfortunately, it was difficult to reliably obtain a single mode spectrum. The merits of a commercially available, blue laser diode package with volume holographic grating optical feedback were explored. I demonstrated that blue-laser diodes that are stabilized by volume holographic gratings have sufficient temporal coherence to pattern diffraction nanostructures over a continuous area greater than 1 cm^2.

Chapter 4

Simple Spatial Filtering

It probably under-scored my emphasis on engineering... If you are making a physical thing and send it to a collaborator, it has to work in other people's hands. It takes the issue of fraud off the table.

John A. Rogers, Former MIT Graduate Student[27]

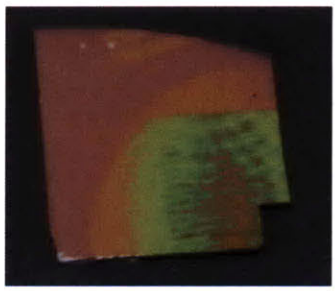

Figure 4-1: Evidence of spatial incoherence on a substrate.

Although the first Tiny Lloyd's Mirror was able to produce nanoscale patterns, often the exposed area was very non-uniform on a macroscopic level. Part of this was the beating problem that was presented in Chapter 3. Another issue was the spatial uniformity of the beam. Often after exposure, I would see substrates that looked like Fig. 4-1. The differences in color are due to differences in topology. In order to eliminate this problem, I explored ways to fix the spatial coherence of the laser beam.

4.1 Spatial Coherence

The theory of interference lithography assumes an ideal incident plane wave of a single frequency. But a beam from a laser, no matter how well collimated, is not an ideal plane wave. A spatial filter (as used in IL) is an optical device that uses the fourier transforming properties of a lens to create a beam of a single transverse mode, TEM_{00}.

Figure 4-2 shows an example of a spatial filtering system. An incident beam is made rectangular by passing the beam through a large aperature. The sharp edges of the rectangle possess many high frequency spatial components. A lens of focal length f is then used to Fourier transform the image of the incident beam at a distance f after the lens. The plane in which the Fourier transform occurs is called the transform plane. Light far from the center corresponds to high spatial frequency components of the image. Light near the center corresponds to low spatial frequency, forward propagating plane waves.

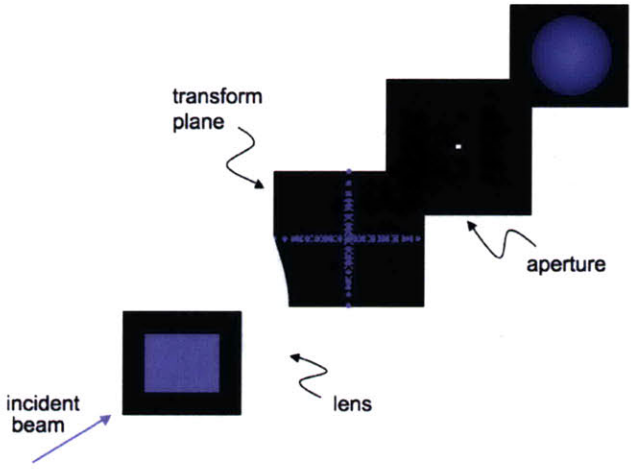

Figure 4-2: Spatial filtering of a square intensity distribution. Light passes through a lens, which creates an image of the Fourier transform of the square. This light is filtered using a pinhole, which emits an Airy Disk intensity distribution.

For a spatial filter, we place a pinhole (a circular aparature) close to the transform plane. If the pinhole is smaller than the beam waist, the pinhole will diffract light, emitting a spherical wave with an Airy Pattern intensity distribution. Far from the pinhole this spherical wave can be approximated as a plane wave.

With IL, the design of a spatial filter must provide two desirables: large patterning area and high exposure intensity. The exposure area is primarily controlled by the pinhole. Small pinholes diffract light at large angles. Therefore small pinholes create larger beams, with more uniform intensity over a given area than large pinholes. Figure 4-3 shows the intensity distribution at the v-block for different pinhole sizes. For a circular aperture, diffraction yields an Airy pattern intensity distribution[24]:

$$I(\rho) = I_0 \left[\frac{2J_1(\chi)}{\chi}\right]^2 \tag{4.1}$$

$$\chi = \left(\frac{2\pi}{\lambda}\right)\left(\frac{D}{2}\right)\left(\frac{\rho}{l}\right), \tag{4.2}$$

where I_0 is the peak intenstiy, $J_1(x)$ is the Bessel function of the first kind of order 1, D is the pinhole diameter, l is the beam expansion length, and ρ is the radial

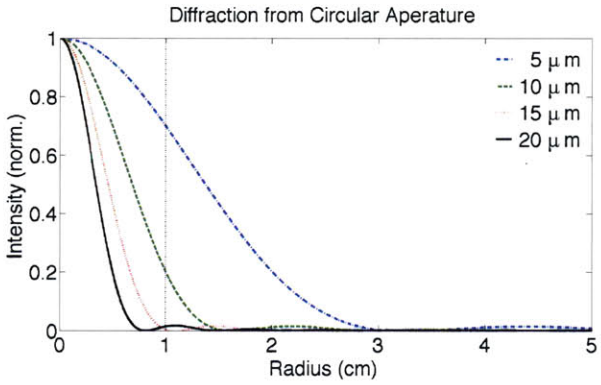

Figure 4-3: Fraunhofer diffraction from a circular aperture. Calculated Airy patter intensity distributions as a result of diffraction from 5, 10, 15, and 20 μm diameter apertures. The plots are for a ~33 cm beam expansion.

distance at the substrate. The calculations were made assuming an ~33 cm beam expansion length. The goal was to create nanostrucutres that extended out 1 cm from the mirror-substrate intersection in hopes of guaranteeing 1 cm^2 of patternable area. Figure 4-3 shows that a 5 μm pinhole has only a -30% drop in intensity over 1 cm. On the other hand, a 10 μm pinhole would create a beam with a -80% decrease.

For a given pinhole, the exposure intensity will be controlled by the focal length of the lens. The radius of the spot of a focused beam from a lens is[24]:

$$r = \frac{1.22\lambda f}{w}, \tag{4.3}$$

where d is the spot size, λ is the wavelength, f is the lens focal length, and w is the width of the beam before entering the lens. Figure 4-4 shows the beam spot size for different focal lengths. The plots are for w = 0.8 mm and 0.4 mm, which are the widths of the major and minor axis of the laser beam. Figure 4-4 demonstrates that smaller focal lengths are beneficial, because creating a smaller spot will allow more of the focal spot to fit through the pinhole.

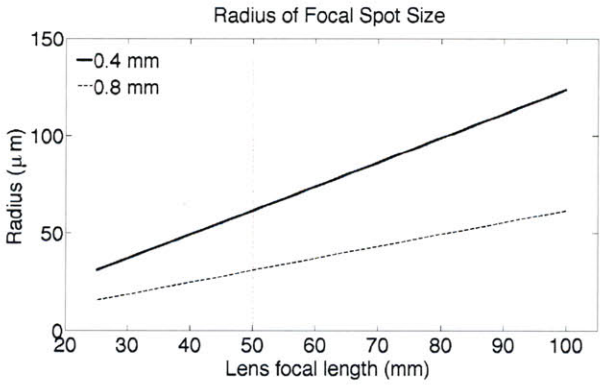

Figure 4-4: Spot size of a focused optical beam. Plotted is the calculated minimum spot size as a function of the lens focal length. The plots are for a 0.4 and 0.8 mm diameter entrance beam.

4.2 Simple Spatial Filtering

After the Tiny Lloyd's Mirror, other research groups became interested in tackling the problem of low-cost interference lithography. For example, Byun et al. were able to use a AlInGaN blue laser diode to make 290 nm pitch gratings and 750 nm pitch two-dimensional rod and hole patterns for ~15 000 USD.[28] Their setup required a spatial filter (which requires training and skill to align) and a 2.2-meter beam-expansion length. My goal was to create a simple spatial filter that required minimal alignment and a short beam expansion length.

I built a low-cost spatial filter from a lens aligned through a lens tube to a pinhole that is mounted on a +/- 1 mm travel, 100 threads-per-inch (TPI) XY lens translating mount. The 0.25 NA lens was mounted within the lens tube, and the translating mount was attached collinearly to the lens tube. The lens focal distance was adjusted with 40 TPI retaining rings to bring the pinhole close to the focal plane, and the 100 TPI screws on the translating mount provided enough control to align the 5-μm-diameter pinhole to the focal spot of the lens. This design made use of the passive linearity and stability of a lens tube to eliminate the tip-tilt stage of more elaborate spatial filters. Beyond the spatial filter, the beam freely expands until it reaches the substrate stage. The distance between the spatial filter and the substrate stage is

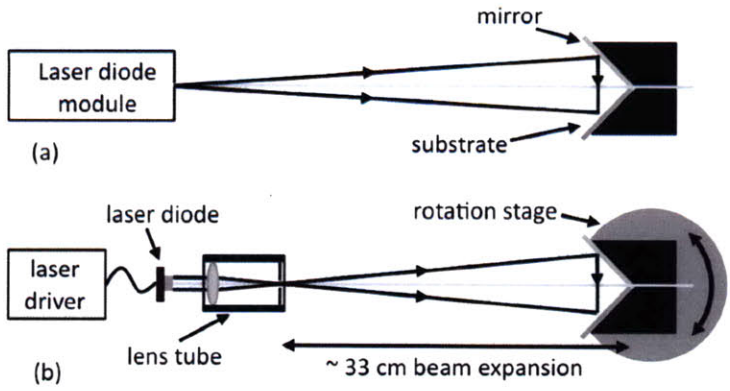

Figure 4-5: Schematics of the first and second Tiny Lloyd's Mirror. (a) The previous setup included a 405 nm laser diode module and an inexpensive mirror/substrate chuck. (b) The new setup includes a laser driver; a collimated, grating-feedback laser diode; a spatial filter consisting of a lens and pinhole inside a lens tube system; an inexpensive mirror/substrate chuck; and a rotation stage. Rotation of the mirror/substrate chuck allows the pitch to be modified. The beam expansion length is ~33 cm.[26]

only 33 cm.

4.3 The Tiny Lloyd's Mirror II

4.3.1 Setup

Using the simple spatial filter and the laser with a volume holographic grating described in Ch. 3, I constructed a new Lloyd's mirror IL tool – the Tiny Lloyd's Mirror II. Figure 4-5 composes schematics of the previous and current setups. A 5 mW, 405 nm laser diode module emitted an expanding beam of light that was aligned to a simple mirror/substrate chuck. The laser-diode current and power were not stabilized nor was there a spatial filter and, moreover, the pitch of the resulting one-dimensional nanostructures was not adjustable. In contrast, Fig. 4-5(b) shows the improved interference lithography system. Improvements include the use of a commercially available 12 mW, 405 nm laser diode package with an integrated collimation and volume holographic grating (VHG) optical feedback system, a shutter/spatial filter assembly that

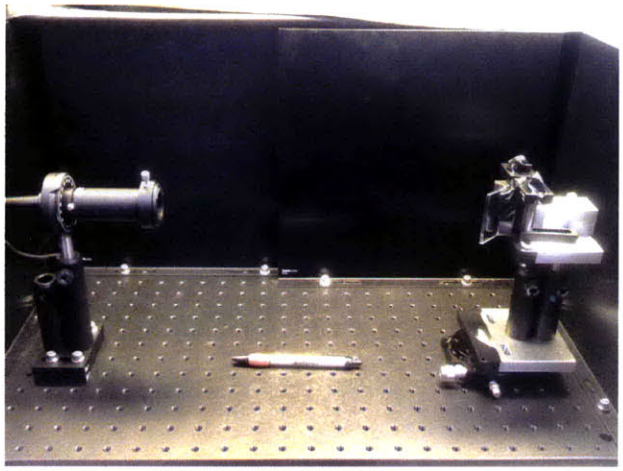

Figure 4-6: Picture of the Tiny Lloyd's Mirror II.

does not require micrometers, and a rotation stage having arc-minute accuracy.

The diode package I used was obtained at a substantially lower cost than more commonly used gas lasers and does not require periodic maintenance or frequent alignment. In contrast to grating- or etalon-based external cavity diode laser systems[29], the embedded VHG makes the IL system easier to configure, because the grating provides a optical feedback system without requiring any external cavity alignment.[25] The diode was mounted in a rotation mount to allow the polarization of the beam to be set with the E-field pointing perpendicular to the plane-of-incidence of the substrate and to allow the laser source to be attached to the beam shutter and spatial filter.

The substrate/mirror mount consisted of a 90° angle machinists v-block connected to a rotation stage with micrometer controlled travel. Rotation of the v-block allowed control of the pitch of the periodic patterns. On one side of the v-block was mounted a 3.5 cm $\times$ 5.0 cm aluminum first-surface mirror with a multi-layer film of dielectrics on top. On the other side was placed the substrate. Both were adhered to the machinist's block with double-sided adhesive carbon tape. Figure 4-6 is a picture of the tool. Together, the proposed tool minimized size, complexity, and cost. The tool had a footprint of only 0.2 m^2. Setup, maintenance, and alignment were simple. Lastly, the tool cost less than 6000 USD.

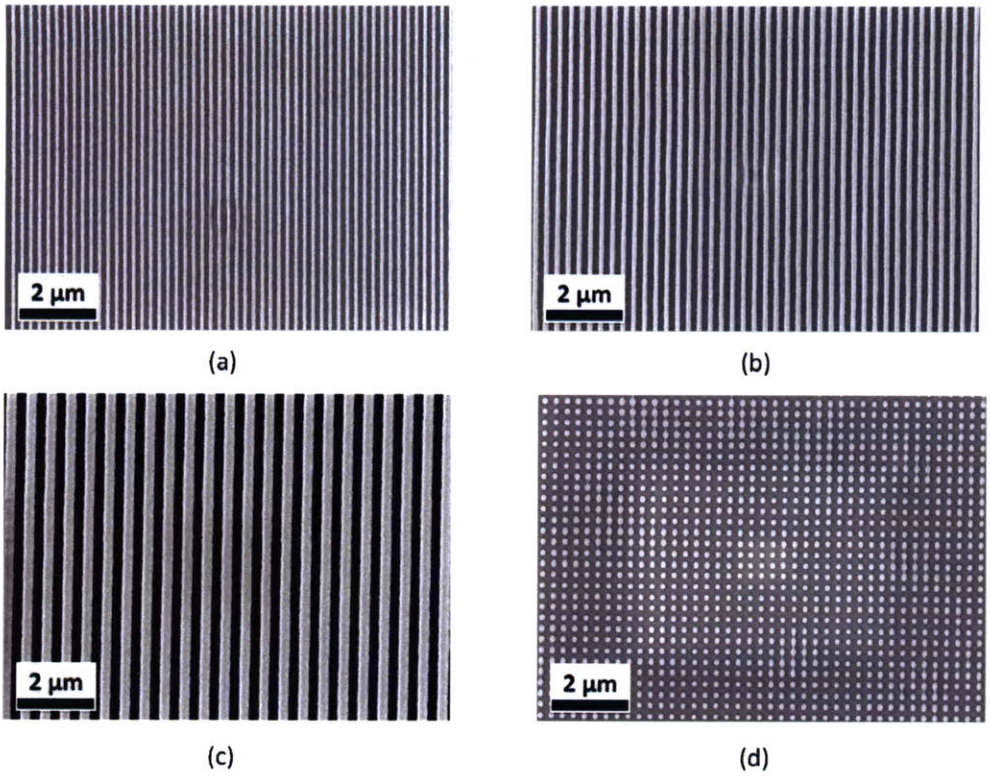

Figure 4-7: Scanning-electron-micrograph images of patterns, produced by the second Tiny Lloyd's Mirror, in positive photoresist. The images were taken at 5 keV electron energy and a working distance of 4 mm. The periods of the patterns are (a) 230 nm, (b) 292 nm, (c) 559 nm, and (d) 314 nm. The figure displays the tool's ability to change the pitch of one-dimensional gratings and to produce two-dimensional patterns.[26]

4.3.2 Results

With the Tiny Lloyd's Mirror II, I was able to accomplish the following results: (1) new patterns were not limited to 1 mm^2 area, (2) the system can modify the pitch of the resulting pattern, and (3) the system has the ability for form two-dimensional patterns.

Figure 4-7 shows periodic nanostructures in photoresist. Figures 4-7(a), (b), and (c) are a set of three gratings at different pitch. The pitches, which were measured in an SEM, were $p_a = 230$ nm, $p_b = 292$ nm, and $p_c = 559$ nm. The angle of exposure is related to the period by the Eqn. 1.1:

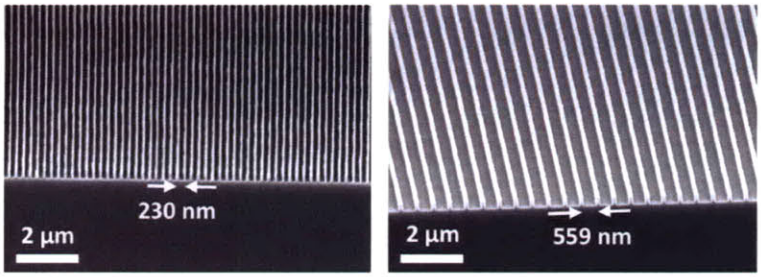

Figure 4-8: One-dimensional periodic patterns transferred into the antireflection coating (ARC) layer. The scanning-electron-microscope images were taken at 5 keV electron energy and 4 mm working distance. The periods were (a) 230 nm and (b) 559 nm.[26]

$$p = \frac{\lambda}{2 \sin \theta}.$$

Using the peak wavelength of the measured laser spectrum (404.9 nm), we find the exposure angles to be $\theta_a = 61.7°$, $\theta_b = 43.9°$, and $\theta_c = 21.2°$.

Figure 4-7(d) shows a two-dimensional rod pattern produced with the Lloyd's Mirror. The pitch of the pattern was 314 nm. There was observable bridging between some of the posts. We attribute this bridging to a spatial intensity variation that may be due to incoherent reflection from our mirror edges or may originate from imperfections of the spatial filter.

Figure 4-8 shows grating lines pattern-transferred into the antireflection coating. Figure 4-8(a) is of 230 nm pitch and is the same substrate as in Fig. 4-7(a). Figure 4-8(b) has a pitch of 559 nm and is the same substrate as Fig. 4-7(c).

4.4 Summary

The critical result of this chapter is the ability to fabricate large-area ($\sim \text{cm}^2$) periodic nanostructures with a simple, compact, low-cost tool. Although existing interference lithography tools can produce periodic nanostructures over 90 cm^2, these tools typically have a $\sim$2.8 m^2 footprint, require significant maintenance, and cost upwards of

100 000 USD. In contrast I have shown that spatially coherent beams can be formed in a simple and compact way using a lens-tube-integrated spatial filter. With only a 0.2 m^2 surface area, the Tiny Lloyds Mirror II is a table-top interference lithography system that requires minimal setup and maintenance. Notably, I have been able to keep the cost of the tool below 6000 USD.

Chapter 5

Future Work

You mean I still have 5 minutes?! Oh, I can slay a lot of dragons in that time.

Cardinal Warde, MIT Professor of Electrical Engineering[1]

[1]Heard many times near the end of lecture for 6.637 (paraphrased).

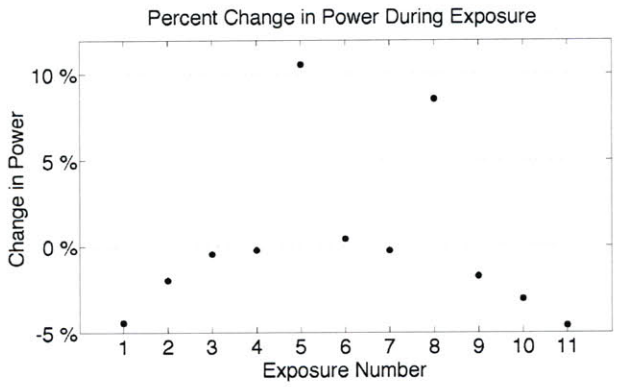

Figure 5-1: Data of the percent change in incident power over an exposure.

The Tiny Lloyd's Mirror project has proven that there is interest and demand for simple, low-cost lithography tools. The challenge was to solve the conflicting demands of functionality and simplicity. The successful development of the Tiny Lloyd's Mirror provides a model to build upon in furthering the goal of achieving ubiquitous low-cost lithography. There are options for future work.

The most pressing issue regarding the Tiny Lloyd's Mirror is that of constant power. Figure 5-1 shows the percent change in power over the duration of an single exposure for a series of exposures. The incident power over a 0.709 cm^2 detector area was measured immediately before and after exposure. Exposures 1-5 were approximately 30-60 seconds long while exposures 6-11 were $\sim$190 sec. The power is observed to often decrease over the exposure time and can vary by up to 10%. Feedback from a photodiode is used in many commercial laser diode housings to maintain constant laser power. A future design of the TLM would incorporate photodiode feedback while still maintaining the simple setup of the lens tube system.

The second opportunity for future contributions is to setup an enclosure. At 12 mW, the laser with volume holographic grating feedback is characterized as a class 3b laser. Although only $\sim$0.8 mW makes it through the 5 μm pinhole, some potential users have expressed safety concerns over the laser power. Creating an enclosure that limits the ability of users to peer directly into the pinhole is desirable. Also developing standard operating procedures for assembly of the system would limit

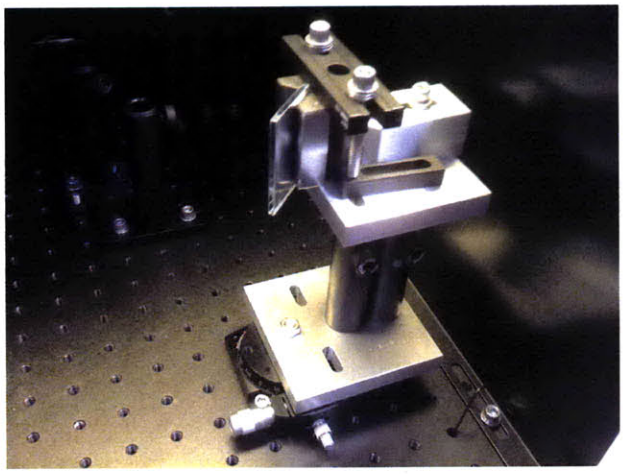

Figure 5-2: Picture of the current setup for the vee block. The vee block is mechanically clamped in place. A rotation stage is used to change the indent angle of exposure. Aluminum spacers are used to position the center of the mirror/substrate axis above the rotational axis.

potential safety hazards.

One part of the design of the Tiny Lloyd's Mirror that was not emphasized was the machinist's vee block setup. Errors in the pitch caused by alignment of the vee block with respect to the axis of rotation and by rotational accuracy are discussed extensively in Walsh's thesis.[3] Figure 5-2 shows the current configuration, which emphasizes ease of setup. Aluminum spacers are used to align the vee block to the rotational axis and the vee block is mechanically clamped. Future designs should focus on a configuration that is more mechanically robust but remains simple, cheap, and accurate.

Lastly, a demonstration of ARC-absent interference lithography with the TLM should be done. Potential users have expressed interest in finding a way to eliminate the need for anti-reflection coating, because ARC adds another layer of complexity in terms of spinning the film and etching through it. Figure 5-3 shows simulation results from the ILSim Matlab program.[30] The graphs are of the latent intensity pattern in PFI-88 photoresist after exposure. In Fig. 5-3(a) there is 180 nm of PFI-88 on top of 25 nm of SiO_x, followed by a silicon substrate. The high intensity area is not vertically continuous, demonstrating that there is a vertical standing wave intensity

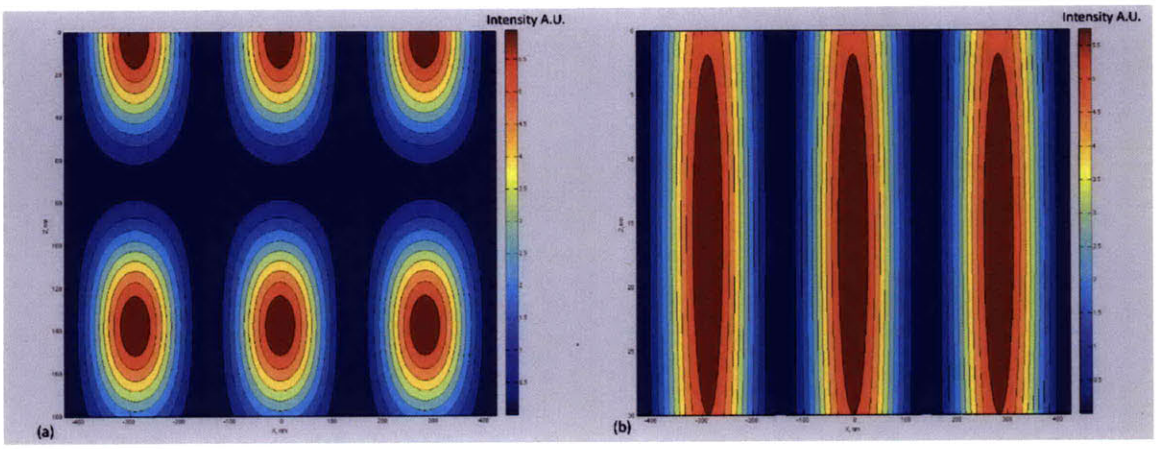

Figure 5-3: Simulation of the latenet intensity pattern in photorestist after exposure. (a) 180 nm of PFI-88, 25 nm of SiO_x and a silicon substrate. (b) 30 nm of PFI-88, 60 nm of SiO_x and a silicon substrate.

pattern. Gratings fabricated with this setup would not develop all the way down to the SiO_x. Figure 5-3(b) shows the intensity distribution for 30 nm of PFI-88 on 60 nm of SiO_x. By thinning the photoresist and tailoring thickness of the SiO_x layer, the standing waves can be minimized.

The elimination of the need for ARC using thin photoresist has been explored at MIT's Nanostructures Laboratory. Recently, a Lloyd's mirror IL setup was used to fabricate a two-dimensional pattern in 44 nm thick PFI-88.[31] In that implementation, the photoresist was spun on a silicon substrate with a native oxide layer. Future work would involve developing a process to show that patterns in thin photoresist can be transferred into the underlying substrate.

Bibliography

[1] Pepper White. *The Idea Factory: Learning to Think at MIT*, page 240. The MIT Press, October 2001.

[2] Juan Ferrera, M. L. Schattenburg, and Henry I. Smith. Analysis of distortion in interferometric lithography. *Journal of Vacuum Science and Technology B*, 14:4009–4013, Nov/Dec 1996.

[3] Michael E. Walsh. *On the design of lithographic interferometers and their applications.* PhD thesis, Massachusetts Institute of Technology, September 2004.

[4] M. L. Schattenburg, R. J. Aucoin, and R. C. Fleming. Optically matched trilevel resist process for nanostructure fabrication. *Journal of Vacuum Science and Technology B*, 13(6):3007–3011, Nov/Dec 1995.

[5] S. R. J. Brueck. Optical and interferometric lithography - nanotechnology enablers. *Proceedings of the IEEE*, 93:1704–1721, Oct 2005.

[6] Y. S. Jung and C. A. Ross. Orientation-controlled self-assembled nanolithography using a polystyrene-polydimethylsiloxane block copolymer. *Nano Letters*, 7:2046–2050, July 2007.

[7] Xian-Zhong Chen and Hai-Ying Li. Fabrication of nanoimprint stamp using interference lithography. *Chinese Physics Letters*, 24:2830–2832, October 2007.

[8] R Menon, H. Y. Tsai, and Thomas S. W. Far-field generation of localized light fields using absorbance modulation. *Physical Review Letters*, 98(043905), January 2007.

[9] Trisha L. Andrew, Hsin-Yu Tsai, and Rajesh Menon. Confining light to deep subwavelength dimensions to enable optical nanopatterning. *Science*, 324:917–921, May 2009.

[10] Edwin Lamers, X. Frank Walboomers, Maciej Domanski, Joost te Riet, Falco C. M. J. M. van Delft, Regina Luttge, Louis A. J. A. Winnubst, Han J. G. E. Gardeniers, and John A. Jansen. The influence of nanoscale grooved substrates on osteoblast behavior and extracellular matrix deposition. *Biomaterials*, 31:3307–3316, April 2010.

[11] Michael E. Walsh. Nanostructuring magnetic thin films using interference lithography. Master's thesis, Massachusetts Institute of Technology, August 2000.

[12] Thomas B. O'Reilly and Henry I. Smith. Photoresist characterization using double exposures with interference lithography. *Journal of Vacuum Science and Technology B*, 26:128–131, Jan/Feb 2008.

[13] John Maeda. *The Laws of Simplicity*, page 2. The MIT Press, September 2006.

[14] Akira Kouchiyama, Katsuhisa Aratani, Yoshihiro Takemoto, Takashi Nakao, Shinichi Kai, Kiyoshi Osato, and Kenzo Nakagawa. High-resolution blue-laser mastering using an inorganic photoresist. *Japanese Journal of Applied Physics*, 42:769–771, February 2003.

[15] Heidelburg Instruments. μPG 101: The tabletop laser pattern generator, June 2009.

[16] C. C. Su, T. C. Wu, J. H. Hsu, S. J. Hwang, and S. H. Chang. Proceedings of the 34th micro and nano engineering conference. 2008.

[17] Corey P. Fucetola, Hasan Korre, and Karl K. Berggren. Low-cost interference lithography. *Journal of Vacuum Science and Technology B*, 27(6):2958–2961, Nov/Dec 2009.

[18] Corey P. Fucetola. Tiny Lloyd's Mirror. 6.781 final project, Massachusetts Institute of Technology, Cambridge, May 2008.

[19] Joseph W. Goodman. *Statistical Optics*, pages 158–164. Wiley Classics Library, New York, 2000.

[20] Karl K. Berggren and Henry I. Smith. Nanostructure Fabrication. 2010.

[21] H. Hemmati. Single longitudinal mode operation of semiconductor laser arrays with etalon feedback. *Applied Physics Letters*, 51:224–225, July 1987.

[22] M. V. Romalis. Narrowing of high power diode laser arrays using reflection feedback from an etalon. *Applied Physics Letters*, 77:1080–1081, August 2000.

[23] Eugene Hecht. *Optics*. Pearson: Addison Wesley, 4th edition, 2002.

[24] Bahaa E. A. Saleh and Malvin Carl Teich. *Fundamentals of Photonics*. Wiley-Interscience, 2007.

[25] Gregory J. Steckman, Wenhai Liu, Rene Platz, Dominic Schroeder, Christophe Moser, and Frank Havermeyer. Volume holographic grating wavelength stabilized laser diodes. *IEEE Journal of Selected Topics in Quantum Electronics*, 13:672–678, May/Jun 2007.

[26] Hasan Korre, Corey P. Fucetola, Jeremy A. Johnson, and Karl K. Berggren. Development of a simple, compact, low-cost interference lithography system. In Review, June 2010.

[27] Robert F. Service. Farewell to flatland. *Science*, 329:138–139, July 2010.

[28] Ikjoo Byun and Joonwon Kim. Cost-effective laser interference lithography using a 405 nm AlInGaN semiconductor laser. *Journal of Micromechanics and Microengineering*, 20(055024), May 2010.

[29] C. E. Wieman and L. Hollberg. Using diode-lasers for atomic physics. *Review of Scientific Instruments*, 62:1–20, January 1991.

[30] Yongfa Fan, Anatoly Bourov, Lena Zavyalova, Jianming Zhou, Andrew Estroff, Neal Lafferty, and Bruce W. Smith. ILSim – a compact simulation tool for interferometric lithography. *Proceedings of SPIE*, 5754:1805–1816, 2005.

[31] Lin Lee Cheong. Low-voltage spatial-phase-locked scanning-electron-beam lithography. Master's thesis, Massachusetts Institute of Technology, Cambridge, June 2010.